

Seasonal Nitrogen Cycles on Pluto

CANDICE J. HANSEN

Jet Propulsion Laboratory, California Institute of Technology, Pasadena, California 91109
E-mail: cj@frostrus.jpl.nasa.gov

AND

DAVID A. PAIGE

Department of Earth and Space Sciences, University of California, Los Angeles, Los Angeles, California 90024

Received March 21, 1994; revised October 27, 1995

A thermal model, developed to predict seasonal nitrogen cycles on Triton, has been modified and applied to Pluto. The model was used to calculate the partitioning of nitrogen between surface frost deposits and the atmosphere, as a function of time for various sets of input parameters. Volatile transport was confirmed to have a significant effect on Pluto's climate as nitrogen moved around on a seasonal time scale between hemispheres, and sublimed into and condensed out of the atmosphere. Pluto's high obliquity was found to have a significant effect on the distribution of frost on its surface. Conditions that would lead to permanent polar caps on Triton were found to lead to permanent zonal frost bands on Pluto. In some instances, frost sublimed from the middle of a seasonal cap outward, resulting in a "polar bald spot". Frost which was darker than the substrate did not satisfy observables on Pluto, in contrast to our findings for Triton. Bright frost (brighter than the substrate) came closer to matching observables. Atmospheric pressure varied seasonally. The amplitudes, and to a lesser extent the phase, of the variation depended significantly on frost and substrate properties. Atmospheric pressure was found to be determined both by Pluto's distance from the sun and by the subsolar latitude. In most cases two peaks in atmospheric pressure were observed annually: a greater one associated with the sublimation of the north polar cap just as Pluto receded from perihelion, and a lesser one associated with the sublimation of the south polar cap as Pluto approached perihelion. Our model predicted frost-free dark substrate surface temperatures in the 50 to 60 K range, while frost temperatures typically ranged between 30 to 40 K. Temporal changes in frost coverage illustrated by our results, and changes in the viewing geometry of Pluto from the Earth, may be important for interpretation of ground-based measurements of Pluto's thermal emission. © 1996 Academic Press, Inc.

INTRODUCTION

A wealth of new data on Pluto has been acquired in the past 20 years. The discovery of CH₄ (Cruikshank *et al.*

1976), and interest in the influence of Charon on a possible Pluto atmosphere, led Trafton and Stern (1983) to investigate the properties of a methane atmosphere and to propose that volatile transport is an important process active on Pluto today. Stern *et al.* (1988) characterized seasonal CH₄ transport as the enabling process by which bright methane polar caps on Pluto could remain bright, even though CH₄ should gradually darken due to various irradiation mechanisms active in the outer solar system (Lupo and Lewis 1980). Binzel (1990) attributed the apparent existence of a bright south polar cap on Pluto to the long-term flow of CH₄ to this pole, on a million-year time scale, due to the precession of perihelion. Stern and Trafton (1984) also analyzed other constituent candidates for Pluto's atmosphere and predicted, on the basis of cosmic abundances, Pluto's cold temperature, and vapor pressure saturation considerations, that N₂ would be the dominant constituent of Pluto's atmosphere. Trafton (1990) modeled and analyzed a continuum of CH₄/N₂ combinations with regard to hydrodynamic atmospheric escape and evolution of Pluto's volatile reservoir. The recent detection of nitrogen on Pluto motivated our evaluation of seasonal nitrogen transport.

The signature of solid nitrogen was identified in Pluto's near IR spectrum in 1992 (Owen *et al.* 1992), and a tenuous atmosphere was detected in 1988 (Elliot *et al.* 1989, Hubbard *et al.* 1990). It has been proposed that Pluto may have a nitrogen-dominated atmosphere in vapor pressure equilibrium with surface frosts (Owen *et al.* 1993). If this is the case, Pluto joins Mars and Triton in possessing a climate controlled by a polar-cap-buffered surface-atmosphere system. On Mars certainly, and probably on Triton, atmospheric pressure varies seasonally as polar caps sublime and condense (Leighton and Murray 1966, Trafton 1984, Spencer 1990, Hansen and Paige 1992, Spen-

cer and Moore 1992). Frost deposit locations and rates of sublimation and condensation are determined by energy balance in the frost deposit, as frost deposit temperature changes and the latent heat of the solid–vapor transition balance incoming solar insolation, emitted thermal radiation, and thermal conduction of heat to and from the sub-surface.

On a body whose atmospheric pressure is determined by vapor pressure equilibrium with surface frosts, volatile conditions as a function of time dominate the climate. Forecasting climate forward or backward in time is impossible without incorporation of volatile processes and the physical properties of the frost itself. Frost properties under the cryogenic conditions of the outer Solar System are not well constrained however. Frost inventory, emissivity, and albedo can take on a large range of possible values. By modeling volatile behavior as these parameters are varied, and comparing the model results with observations, we seek to constrain these frost properties.

It is interesting to study Triton and Pluto as a pair, in the context that they may be the surviving representatives of a class of small planets that may have had a similar origin early in the history of the Solar System (Stern 1991). Model predictions may be compared to observables on both Triton and Pluto. Both Triton and Pluto have a volatile inventory which includes N_2 , CH_4 , and CO (Cruikshank *et al.* 1984, Cruikshank *et al.* 1991, Cruikshank *et al.* 1993, Owen *et al.* 1992). Both have thin atmospheres dominated by nitrogen (Broadfoot *et al.* 1989, Tyler *et al.* 1989, Elliot *et al.* 1989, Hubbard *et al.* 1990, Owen *et al.* 1993). Both exhibit bright south poles, from which one might expect frost to have sublimated (Stansberry *et al.* 1990, Hansen and Paige 1992), as both bodies have experienced sunshine at southern latitudes during this epoch. The two bodies have similar size, density, rotational periods, and, when Pluto is at perihelion, their distance from the sun is comparable.

PLUTO OBSERVATIONS

Impressive data sets have been acquired for Pluto by Earth-based observers. Disk-integrated brightness and rotational lightcurves have been measured. Observations of the secular decrease in Pluto's brightness and accentuation of its rotational lightcurve since 1955 are summarized in Stern *et al.* 1988. Early data is clearly consistent with a bright south polar cap. The recent series of Pluto–Charon mutual events have yielded albedo maps of Pluto's surface (Young and Binzel 1993, Buie *et al.* 1992). These maps show a bright south polar region, a dark mid-southern latitude region, and a bright mid-northern latitude region. They differ in whether or not there is a bright or a dark region at higher northern latitudes. Reduction of the lightcurve history combined

with mutual event data by Drish (Drish *et al.* 1995) yields some variation in the albedo map obtained, and confirms theoretical arguments that Pluto's surface albedo distribution has not been static over the past 40 years. The most recent data, images of Pluto obtained by Stern *et al.* (1995) from the Hubble Space Telescope, show a bright north polar cap.

A fortuitous stellar occultation in 1988 enabled the detection of Pluto's tenuous atmosphere. Although there is some controversy in interpretation of the data within a scale height of the surface, measurement of Pluto's atmospheric pressure was possible. Assuming that nitrogen is the dominant constituent, the pressure is roughly on the order of 0.2 to 0.5 Pa (Elliot *et al.* 1989, Hubbard *et al.* 1990, Elliot and Young 1991).

Pluto's disk-integrated brightness temperature has been measured both at far IR (Sykes *et al.* 1987) and at millimeter wavelengths (Altenhoff *et al.* 1988, Stern *et al.* 1993, Weintraub *et al.* 1993). The data was acquired at different times, and does not give the same brightness temperature at different wavelengths. Wavelength dependent emissivity seems to be required in order to reproduce these observations with simple thermal models (Sykes 1993).

The challenge now is to pull all these observations together into a general picture of what may be taking place on Pluto's surface and atmosphere. To do this one must disentangle temporal variability due to changes in the observing geometry of Pluto from the Earth, from changes due to volatile transport. Our approach to this is to apply a thermal model to Pluto's seasonal nitrogen cycle.

There are two valuable results which come from modeling a problem. First is the capability to analyze trends as parameters are varied. This trend analysis can be used in our application to constrain frost properties. The second important capability is to pin down a set or sets of parameters consistent with Pluto observations, and then proceed to address specific questions relevant to understanding surface properties and volatile transport on the planet.

The Pluto questions which we wish to address with our model are as follows:

1. Can Pluto observations be described in terms of an N_2 atmosphere in vapor pressure equilibrium with surface frost deposits?
2. How does Pluto's eccentric orbit and high obliquity affect its volatile distribution with time?
3. What surface and frost temperatures are likely, as a function of time, for a body at Pluto's distance from the sun?
4. What atmospheric pressures are likely, and how do they vary seasonally? Can we bound a range of possible atmospheric pressure levels and variation for planning purposes for Pluto mission opportunities?

5. What insights gleaned from modeling volatile behavior on Pluto are applicable to Triton? As input parameters are varied, do we note the same trends in volatile partitioning and distribution as previously determined for Triton (Hansen and Paige 1992)? Can a comparison of Pluto and Triton shed light on the Triton bright frost/dark frost enigma (Spencer 1990, Stansberry *et al.* 1990, Eluszkewicz 1991, Hansen and Paige 1992, Duxbury and Brown 1993)?

THE PLUTO THERMAL MODEL

We have adapted our Triton thermal model to apply to Pluto. Hansen and Paige (1992) originally modified a Mars thermal model to apply to conditions on Triton. This thermal model is based on the successful Leighton and Murray (1966) diurnal and seasonal formulation of the heat balance of the CO₂ polar caps on Mars. The model solves the frost energy balance equation to calculate sublimation and condensation rates as a function of time and latitude. The primary input parameters are the albedo and emissivity of the frost, the albedo and thermal inertia of the substrate, and the total nitrogen inventory. The model outputs frost deposit locations as a function of time, which can be compared to albedo boundaries observed on Pluto, and atmospheric pressure and disk-integrated brightness and temperature, which can be directly compared to earth-based measurements of these quantities on Pluto. Our model dovetails nicely with Trafton's (1990) model, in that we address at a detailed level areas in which he was forced to make simplifying assumptions, namely nonuniform surface frost coverage and albedo distribution, thermal capacity and conductivity of the surface, and seasonally variable frost temperature.

The thermal model used for Pluto is a direct adaptation of the Triton thermal model described in detail by Hansen and Paige (1992). Briefly, the Pluto thermal model solves the heat balance equation shown in Fig. 1 four times per Pluto hour at 18 latitudes. Frost is sublimed or condensed locally at a rate consistent with maintaining global vapor pressure equilibrium, and conservation of mass and energy. The model transitions from a state in which an atmosphere exists and frost temperature changes are controlled by vapor pressure equilibrium, to an atmosphereless state in which little or no latent heat is available, and frost temperature changes are dominated by radiative balance. Transport of heat to and from the substrate, and in substrate layers, is an essential feature for realistic determination of the frost energy balance (Paige, 1992).

The heat balance equation is illustrated in Fig. 1. Solar radiation, S_0 W/m², is absorbed by the surface or frost in an amount dependent on its Bond albedo, A : energy absorbed is $S_0(1 - A)$. Infrared radiation, $\epsilon\sigma T^4$, where ϵ

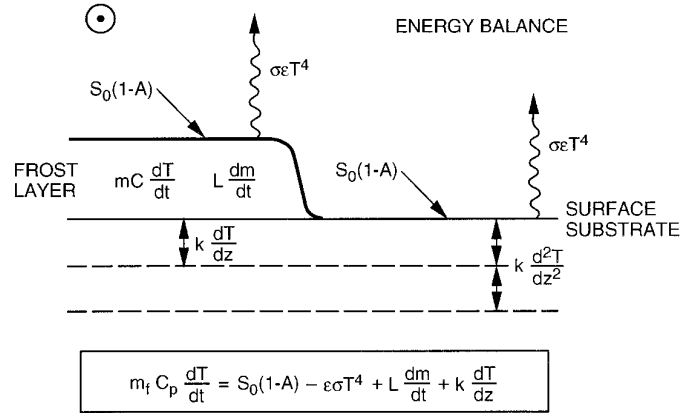


FIG. 1. This figure illustrates the frost heat balance equation solved by the model. A change in frost temperature, $mC dT/dt$, is determined by the combination of incoming solar energy, $S_0(1 - A)$, the emitted thermal energy, $\epsilon\sigma T^4$, latent heat of frost sublimation or condensation, $L dm/dt$, and thermal conduction of heat to and from the substrate, $k dT/dz$. The change in frost temperature is balanced with frost condensed or sublimed in such a way as to insure conservation of energy and global vapor pressure equilibrium.

is emissivity of the frost or surface, σ is the Stefan-Boltzmann constant, and T is the temperature, is emitted. Heat, $k dT/dz$ is conducted to and from subsurface layers, where k is the thermal conductivity of the substrate and dT/dz represents the thermal gradient between the frost and substrate. Below the surface heat transport is treated as a diffusive process, and is proportional to the thermal diffusivity and the second partial derivative, d^2T/dz^2 . Latent heat, L , and the heat capacity of the frost deposit, mC (m is mass in kg/m², C is the specific heat), control frost condensation and sublimation rates, dm/dt , and the rate of change of frost temperature, dT/dt .

Each time this equation is solved there are two unknowns, dm/dt and dT/dt . There is however, one additional constraint, which is that the frost be in solid-vapor equilibrium with the surrounding atmosphere. Therefore, at any given latitude or time, there is a unique combination of values for dm/dt and dT/dt such that the change in frost temperature, the amount of frost sublimed or condensed, and the frostpoint temperature that corresponds to the newly calculated atmospheric pressure are consistent with local conservation of energy, global mass conservation, and vapor pressure equilibrium.

Table I lists some of the most important variables in the model and shows again the considerable degree of similarity between Triton and Pluto. It was not necessary, for example, to change the interior heat flux, which was set to 6 mW/m² for Triton—the similar densities of the two bodies would lead one to predict similar rock content (Null *et al.* 1993, Brown *et al.* 1991). Likewise, the rotational periods are close enough that the depth of the diurnal

TABLE I
Modeling the Pluto–Triton Pair

Characteristic	Triton	Pluto	Model significance
Radius (km)	1350	1150	
Density (kg/m ³)	2080	2129	Assume similar rock content leads to similar internal heat flow
Surface gravity (m/sec ²)	0.79	0.68	
Sidereal period (years)	163.7	248.0	Somewhat similar seasonal thermal wave depth
Rotational period (days)	5.58	6.39	Very similar diurnal thermal wave depth
Volatiles detected in surface ice	N ₂ , CH ₄ , CO, CO ₂	N ₂ , CH ₄ , CO	Assume N ₂ is dominant volatile
Atmospheric pressure (Pa)	1.6	0.2 to >0.5	Model should predict for 1988–1989
Albedo range	0.6/0.9	0.2/0.9	

thermal wave is similar, thus the algorithm used to determine the thicknesses and the number of layers in the substrate could be left unchanged. The top three layers are set to 1/4 the depth of the diurnal thermal wave, with subsequent layers thickening by a factor of 1.13, and we are using 60 layers.

The atmosphere is assumed to be transparent to radiation, and atmospheric pressure is determined by subtracting the amount of N₂ condensed on the surface from the total N₂ inventory assigned. The total N₂ inventory is assumed to be constant over time, although Trafton (1990) has calculated that atmospheric loss due to hydrodynamic escape could be significant even on seasonal time scales. The frost deposit is assumed to be isothermal, which is equivalent to assuming that the frost is porous enough to remain in vapor pressure equilibrium with the atmosphere.

The model makes predictions based on pure nitrogen frost. Nitrogen is by far the dominant volatile constituent, with CO and CH₄ present only in trace amounts (Owen *et al.* 1993), however at present this must be viewed as a serious limitation of the model, which will be discussed in the “Multicomponent Ices” section.

The Pluto thermal model tracks whether nitrogen is in its α or β state. This is a significant change from the Triton model. Solid nitrogen undergoes a phase transition at a temperature of 35.61 K from a hexagonal crystal structure ($T > 35.61$ K) to a cubic structure ($T < 35.61$ K). The model now stops its normal routine when the transition temperature is reached and devotes all energy to the latent heat of the α – β transition, 8180 J/kg (Johnson, 1960). Frost temperature remains constant and no frost is allowed to sublime or condense until the transition from α to β or β

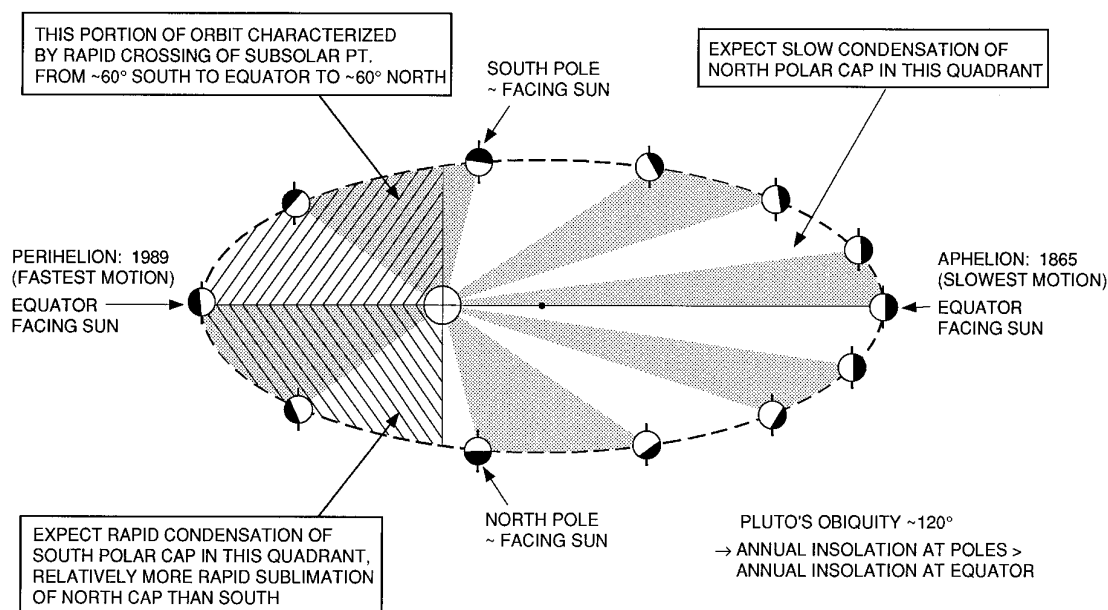


FIG. 2. Pluto's seasons. Pluto's eccentric orbit is expected to affect deposition and sublimation rates of its polar caps.

to α is complete. The model tracks whether frost is in its α or β state at all times. The latent heat of the solid–vapor transition is the appropriate value for the phase of the solid: 2.5×10^5 J/kg for β frost, and 4.3×10^5 J/kg for α frost (Brown and Ziegler 1980).

Pluto's orbit and obliquity enter into the solar insolation term in the heat balance equation. Pluto's orbit is the least circular of all the planets in the Solar System, with an eccentricity of 0.249. Its obliquity is high, 119.998° (derived from Null *et al.* 1993), equivalent to 60° for a prograde-rotation planet. Planets that have obliquities greater than approximately 54° have annual insolation at the poles that is greater than the annual insolation at the equator (Ward 1974). Currently Pluto's orbit orientation is such that the Sun crosses Pluto's equator at perihelion and aphelion.

One might expect that this would affect seasonal frost deposition patterns, as illustrated in Fig. 2, and this expectation is borne out by model results.

An interesting complexity on Pluto is the regime in which volatile transport is supersonic under certain conditions when the atmosphere has nearly completely condensed onto the surface. The model handles this case robustly, in that the frost temperature changes will be calculated in the frost heat balance equation with $L dm/dt$ equal or nearly equal to zero. In this case frost temperatures may begin to diverge, responding to local differences in the other terms in the heat balance equation. Nitrogen may still enter the atmosphere, at cap edges still obliquely illuminated and sublimating. This nitrogen moves poleward, but its latent heat is insufficient

TABLE II
Thermal Model Runs

Run # (kg/m ²)	Thermal inertia ($\times 10^{-3}$ cal/K cm ² sec ^{1/2})	Substrate albedo	Frost albedo	Frost emissivity	N ₂ inventory
4	1	0.8	0.2	1.0	50
1	7	0.8	0.2	1.0	50
2	7	0.8	0.2	1.0	100
6	7	0.8	0.2	1.0	100
3	7	0.8	0.2	1.0	200
5	50	0.8	0.2	1.0	50
16	1	0.4	0.8	0.6	50
11	7	0.4	0.8	0.6	50
17	7	0.4	0.8	0.8	50
18	1	0.4	0.8	1.0	50
13	1	0.3	0.9	0.8	50
23	1	0.2	0.8	0.2	50
20	1	0.2	0.8	0.2	50
34	1	0.2	0.8	0.6	50
31	1	0.2	0.8	0.8	50
33	1	0.2	0.8	1.0	50
37	1	0.2	0.8	0.6	100
38	1	0.2	0.8	0.8	100
41	1	0.2	0.8	0.8	200
24	7	0.2	0.8	0.2	50
21	7	0.2	0.8	0.4	50
35	7	0.2	0.8	0.6	50
12	7	0.2	0.8	0.8	50
30	7	0.2	0.8	1.0	50
43	7	0.2	0.8	0.6	100
15	7	0.2	0.8	0.8	100
40	7	0.2	0.8	0.8	200
42	14	0.2	0.8	0.8	50
19	28	0.2	0.8	0.8	50
25	50	0.2	0.8	0.2	50
22	50	0.2	0.8	0.4	50
36	50	0.2	0.8	0.6	50
14	50	0.2	0.8	0.8	50
32	50	0.2	0.8	1.0	50

to prevent temperatures from plummeting rapidly. Any atmosphere at this time is no longer global, but is localized in the vicinity of the frost deposits, in a manner analogous to Io (Ingersoll 1989).

Model Runs

Over 50 different cases have been run for Pluto. Representative cases are shown in Table II. The primary input parameters varied between runs are substrate albedo and thermal inertia, frost albedo and emissivity, and total nitrogen inventory. All properties remain constant with time within a run and no hemispheric differences have been assigned in runs to date.

On Pluto, as determined from the series of mutual events, surface (geometric) albedo varies from a low of 0.15 to a high of 0.9 (Buie *et al.* 1992, Young and Binzel 1993). Most of the model runs assigned a (Bond) albedo of 0.2 to frost-free substrate and 0.8 to the frost, with a few runs with higher albedos. Some runs assigned 0.8 to the substrate and 0.2 to the frost. As on Triton we wanted to test a “dark frost” hypothesis, although it is harder to imagine a dark frost with an albedo of 0.2 than it was to imagine a frost on Triton that was just relatively dark, with an albedo of 0.6.

Substrate thermal inertia was assigned values of 1, 7, or 50×10^{-3} cal/cm² K sec^{1/2}. A thermal inertia of 0.001 is similar to that derived for Rhea (Spencer and Moore 1992), and estimated for surfaces of fine-grained icy satellites (Morrison and Cruikshank 1973); a thermal inertia of 0.050 is appropriate for solid water ice. Table III gives the depth of the diurnal and seasonal thermal waves for each of these three values.

Frost emissivity was varied from 0.2 to 1.0. Atmospheric pressure is a strong function of frost emissivity for a given Bond albedo (Trafton and Stern 1983, Nelson *et al.* 1990), and thus the range of emissivity/Bond albedo combinations modeled could be constrained by observed atmospheric pressure. Frost-free surface emissivity was varied for a few runs to test its effect on results.

The globally averaged nitrogen inventory was set at either 50, 100, or 200 kg/m². This very important parameter is poorly constrained (Cruikshank *et al.* 1984, Duxbury and Brown 1993). On Triton, to match the spectral data, the minimum inventory could be as little as 10 cm depth over a substantial fraction of the surface if the frost forms a glaze (Grundy *et al.* 1993), or tens of centimeters if not (Cruikshank *et al.* 1984). At the high end, Cruikshank *et al.* (1984) calculated from the solar abundance of nitrogen, and considerations of outgassing and volatile loss using Titan as an analog, that Triton could have a layer of nitrogen up to 1 km in depth. Theoretical work done by Hunten and Watson (1982) and Trafton (1990) on Pluto, given the

TABLE III
Depths of the Diurnal and Seasonal Thermal Waves for Different Thermal Inertias of the Substrate

Thermal inertia ($\times 10^{-3}$ cal/(cm ² sec ^{1/2} K)	Diurnal thermal wave depth (m)	Seasonal thermal wave depth (m)
1	0.02	2.1
7	0.12	15
50	0.88	105

possibility that the ice evaporates and experiences hydrodynamic escape, can be used to infer a starting inventory 1 to 3 km deep.

Model Results

Model output is shown in the figures that follow. All data is plotted as a function of time from 1000 to 2100 A.D. The top panel gives Pluto’s distance from the Sun in AU for reference. Pluto’s highly eccentric orbit is obvious. The second panel plots whole disk albedo. This is simply a sum of surface area with and without frost, weighted by the cosine of the angle from the surface normal, as Pluto would have been viewed from the Earth.

The third panel gives temperatures. Figure 4 and subsequent figures plot four temperatures. (Figure 3 has a different convention than subsequent figures and use of this panel is described in the caption.) The solid line is the calculated frost physical temperature. This has a direct correspondence with atmospheric pressure due to the constraint of maintaining vapor pressure equilibrium. The fine-dotted line is the warmest surface physical temperature of the substrate, anywhere on the planet, at the given time. The dot-dash line gives the disk-integrated brightness temperature that would be observed at the Earth at a wavelength of 60 μ m. The dashed line gives the disk-integrated brightness temperature that would be observed at 1300 μ m. These two temperatures are determined by calculating the emitted flux for each element visible from the Earth, based on the physical temperature calculated in the heat balance equation, and the emissivity.

The fourth panel shows atmospheric pressure as a function of time in pascals on a log scale. Once the atmospheric pressure has dropped below approximately 10^{-4} Pa, the atmosphere has become supersonic, i.e., a sublimation-mass-flux-driven pressure gradient could theoretically build up which would require velocities greater than the speed of sound to redistribute N₂. (As atmospheric density

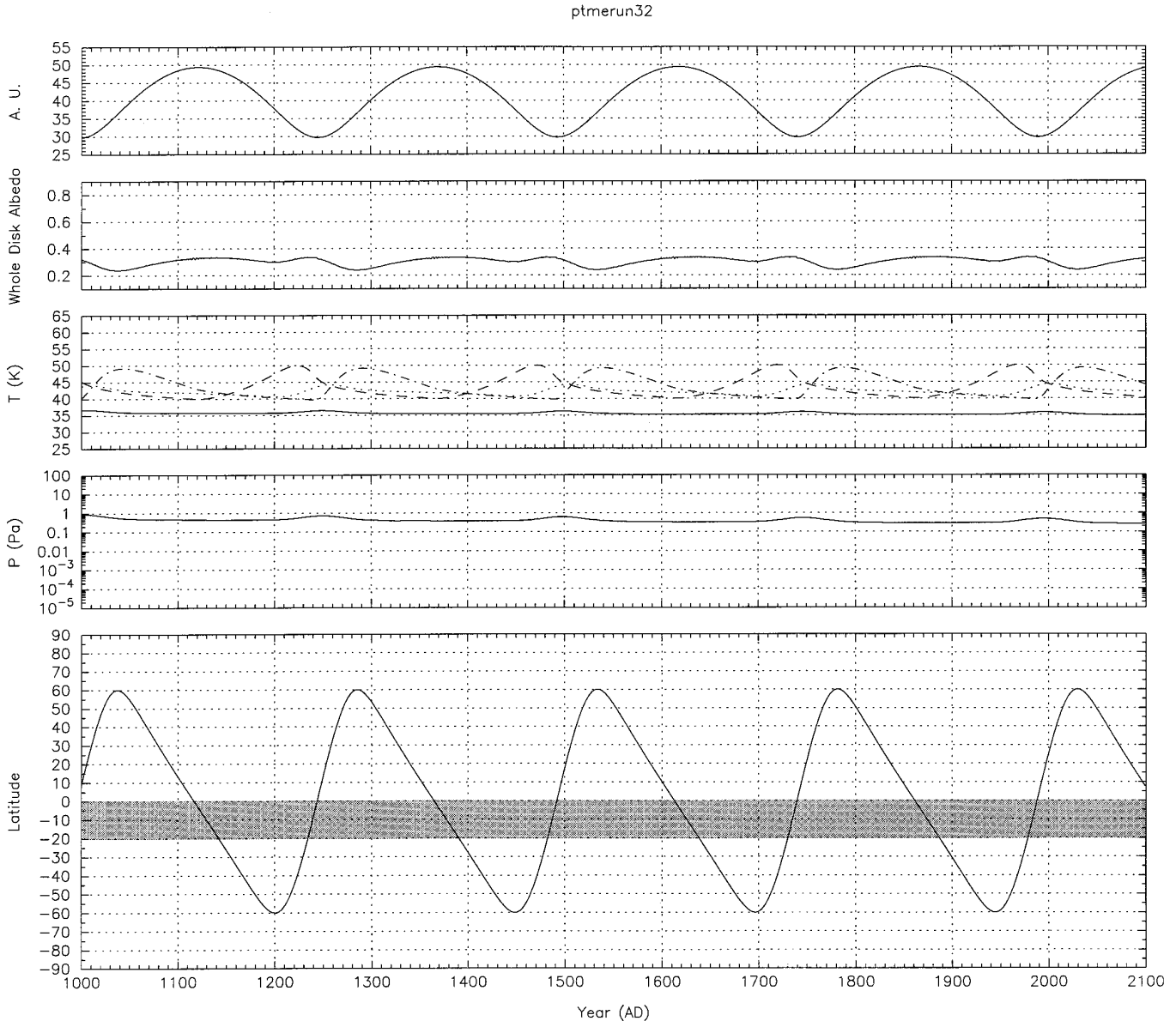


FIG. 3. Model output for a high thermal inertia case (run #32) is shown in this figure. This run had a thermal inertia of $50 \times 10^{-3} \text{ cal/cm}^2 \text{ sec}^{1/2} \text{ K}$, a substrate albedo of 0.2, a frost albedo of 0.8, a frost emissivity of 1.0, and a global N_2 inventory of 50 kg/m^2 . This case predicts the formation of a permanent zonal band of frost. The latitude at which the band is formed is not significant—the latitude is determined by Pluto’s season at the time a run is started. Atmospheric pressure is very stable as frost is immobilized in the permanent band. Temperatures plotted in the third panel are the frostpoint temperature (solid line), the north and south pole temperatures (dash and dash-dot lines), and the temperature at $+10^\circ$ latitude (fine dot). This illustrates why there are no seasonal polar caps—the polar temperature is never low enough for frost to condense. Peaks in the substrate temperature are observed to correspond to maximum excursions of the subsolar point.

decreases, velocity must increase to maintain the same mass flux.) Beyond this point, the atmospheric pressure plotted is the equivalent average global pressure. It is the correct average due to conservation of mass in the model, but most of the atmosphere will be localized in the vicinity of the polar cap.

The bottom panel shows the latitudes at which frost

deposits occur as a function of time. The stippled area is the area predicted to be covered by frost. The sawtooth curve plotted in this panel is the subsolar latitude. It is a sawtooth curve because of Pluto’s eccentricity: the Sun crosses from -60° to $+60^\circ$ latitude quickly as Pluto moves through perihelion, but crosses from $+60^\circ$ to -60° slowly as Pluto moves through aphelion.

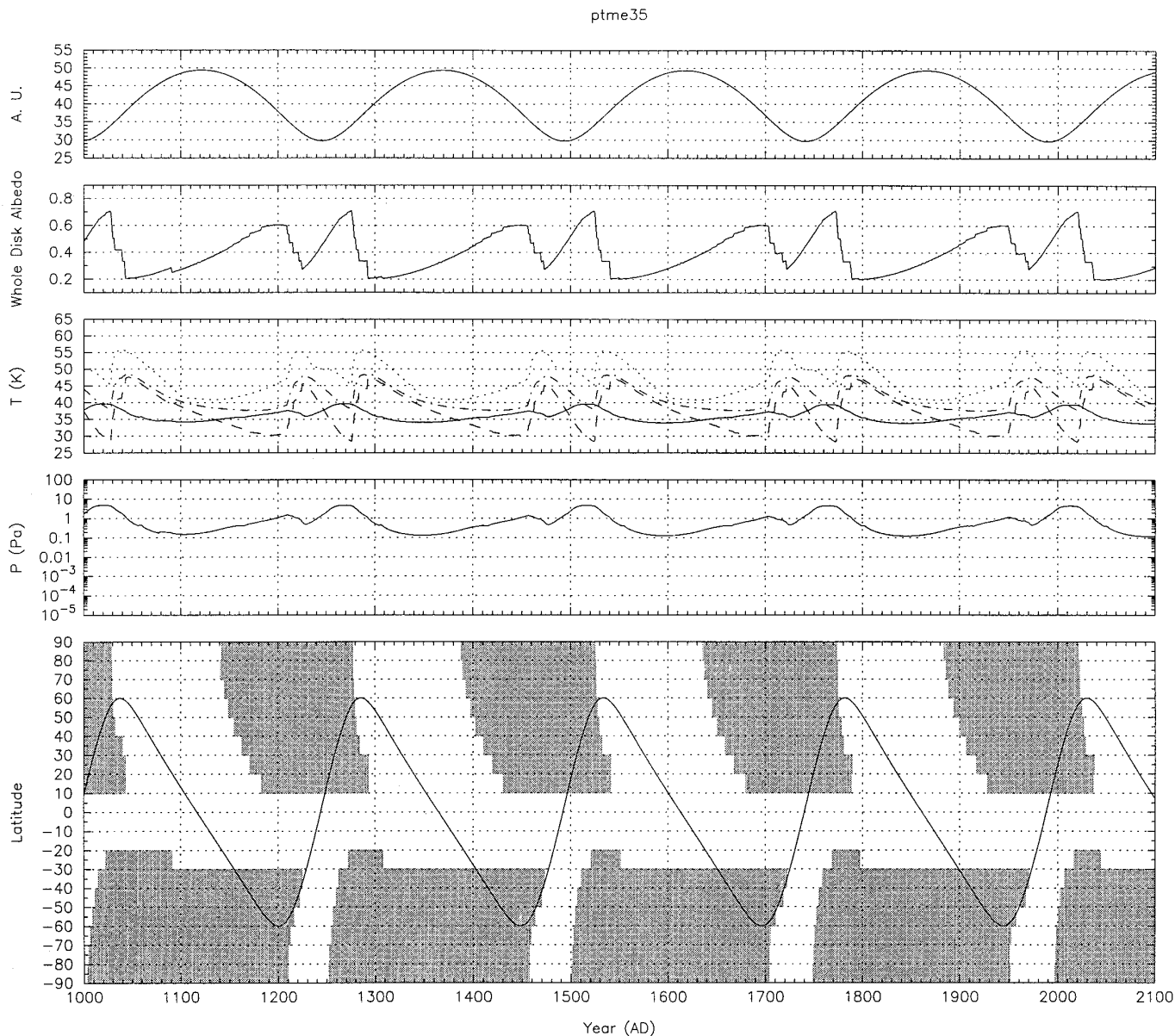


FIG. 4. This case illustrates what happens when the substrate is assigned a moderate thermal inertia (7×10^{-3} cal/cm² sec^{1/2} K). In this run (#35) the substrate albedo was 0.2, the frost albedo was 0.8, the frost emissivity was 0.6, and the global N₂ inventory was 50 kg/m². Polar caps develop, but sublime from the center out, thus developing polar bald spots. The south polar cap is observed to last much longer than the north polar cap, as Pluto moves through aphelion. Two peaks in atmospheric pressure are observed per Pluto year, with the one following perihelion being more pronounced. In this particular case, the next maxima is reached just after 2000 A.D., and persists to ~2020. The temperature curves show that there will be times that the brightness temperature of Pluto measured from the Earth will be dominated by the thermal signature of the frost deposit.

TRENDS

Thermal Inertia

High thermal inertia. All bright frost runs with a high thermal inertia substrate formed permanent zonal bands rather than polar caps (see Fig. 3). This was clearly the result of Pluto's high obliquity. On a seasonal time scale,

higher thermal inertia surfaces required longer to cool off or to warm up, thus remained closer to their annual average temperatures. As noted, Pluto's annual average insolation is higher at its poles than at its equator because of its obliquity. The exact latitude zone at which the band formed was not significant—it depended on the Pluto season at which the run was initiated. (This was

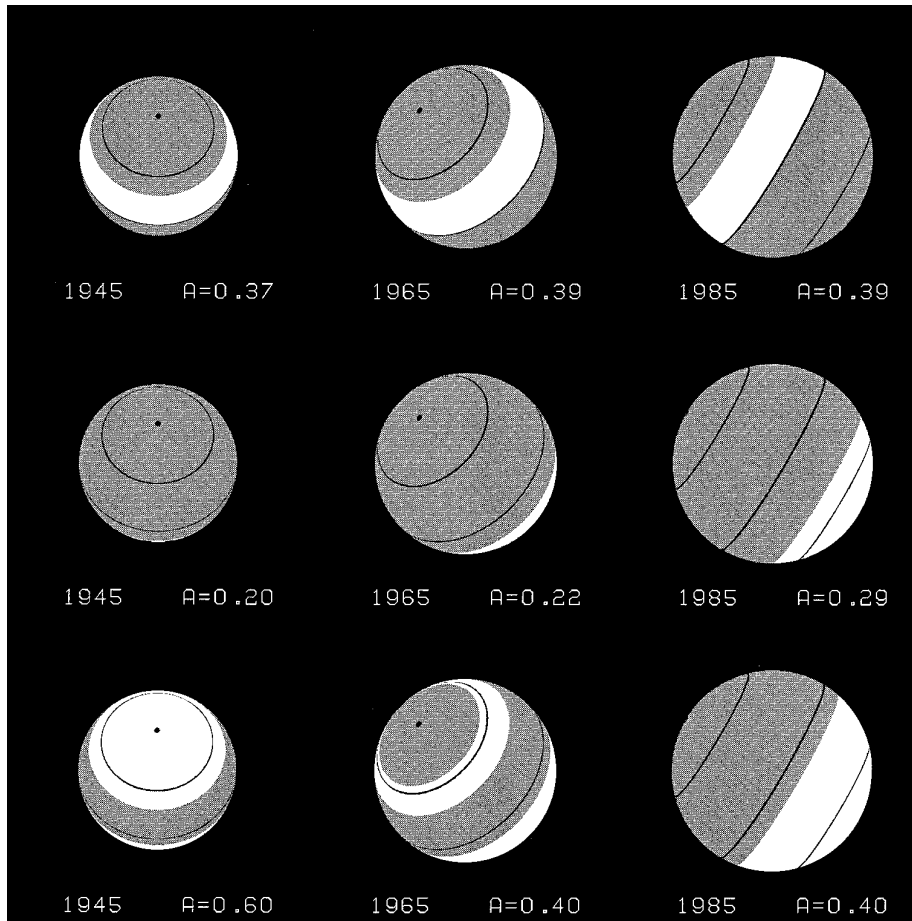


FIG. 5. This figure compares high, low, and moderate thermal inertia cases (top, middle, and bottom panels, respectively) at three different times. South is shown up on this retrograde planet to facilitate comparison to Earth-based data. In this figure, frost covered areas are white and frost-free substrate is dark, in contrast to the convention used for the other figures in which stippling is used to indicate frost coverage. It is clear that both temporal changes in viewing geometry and temporal changes in frost distribution will affect observations. The moderate thermal inertia case gives the best match to observations.

determined by initiation of the same run at different times during the Pluto year). The zonal bands were permanent because the high thermal inertia substrate warmed up and then stayed warm at the poles, due to the higher insolation, preventing the condensation of new frost. The albedo difference between a dark, heat-absorbing substrate and a bright reflective frost further reinforced the stability of the zonal band. Frost temperature was very stable, remaining very close to 35 K in this particular run, thus flattening out seasonal variations in atmospheric pressure. The surface temperature of frost-free substrate reached 50 K when the subsolar point reached its most extreme latitude.

Moderate thermal inertia. Moderate thermal inertia runs with a low nitrogen inventory predicted seasonal polar caps. In many cases these seasonal caps sublimated from the pole out, developing a polar bald spot (see Figs. 4 and 5). The polar caps were asymmetric: the south polar cap

persisted through the slow excursion through aphelion, while the short-lived north polar cap was in place during perihelion.

Substrate temperatures were calculated to reach 55 K, while the frost temperature stayed between roughly 34 and 40 K. High temperatures were correlated with extreme subsolar latitude. The disk-integrated brightness temperature predicted at $1300\ \mu\text{m}$ is observed to dip below the frost temperature—this was due to the frost emissivity, which for this run was set to 0.6.

Some cases were transitional in nature, with a permanent zonal band and seasonal polar caps. This generally happened for moderate inertia cases when the frost was cold, as is the case for a high emissivity or high albedo frost. High inventories of nitrogen also led to this configuration, as shown in Fig. 6, which was a low thermal inertia case. Some frost was mobile enough to sublime and condense into and out of the atmosphere, and to move around sea-

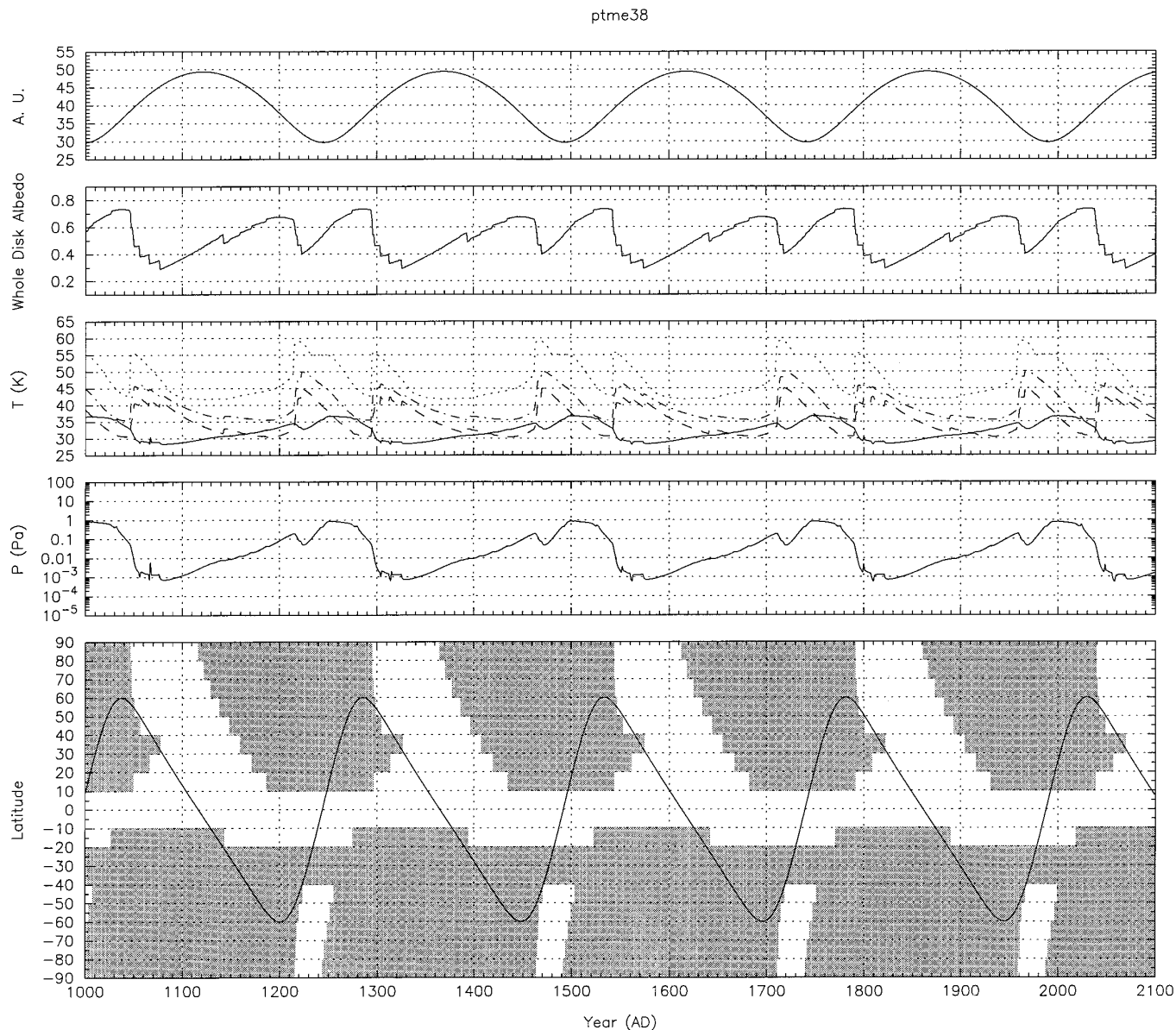


FIG. 6. Sometimes transitional cap/band cases are observed, usually in the case of a cold (high albedo or high emissivity) frost. This configuration also occurs with a relatively large N_2 inventory. The case shown here is run #38, which had a thermal inertia of 1×10^{-3} cal/cm² sec^{1/2} K, a substrate albedo of 0.2, a frost albedo of 0.8, a frost emissivity of 0.8, and a nitrogen inventory of 100 kg/m². A permanent zonal band forms but the frost is still mobile enough seasonally to form seasonal polar caps.

sonally and form polar caps, but the rest remained in the stable zonal band. Seasonal differences in atmospheric pressure were subdued relative to the large difference in pressure associated with (but offset from) perihelion and aphelion.

Low thermal inertia. Low thermal inertia cases with low nitrogen inventories, and all dark frost runs, formed seasonal polar caps. These caps condensed earlier and sublimed earlier than moderate inertia cases (see Fig. 7). Seasonal variation in atmospheric pressure was most pro-

nounced for low thermal inertia runs. Two pressure peaks per Pluto year were predicted. The two atmospheric pressure minima were directly correlated to the condensation of the northern and southern caps. The pressure peak associated with the sublimation of the southern cap as Pluto approached perihelion was typically lower than that associated with the sublimation of the northern cap as Pluto receded from perihelion.

The highest surface temperature of frost-free substrate was predicted to reach 60 K. The frost temperature in this

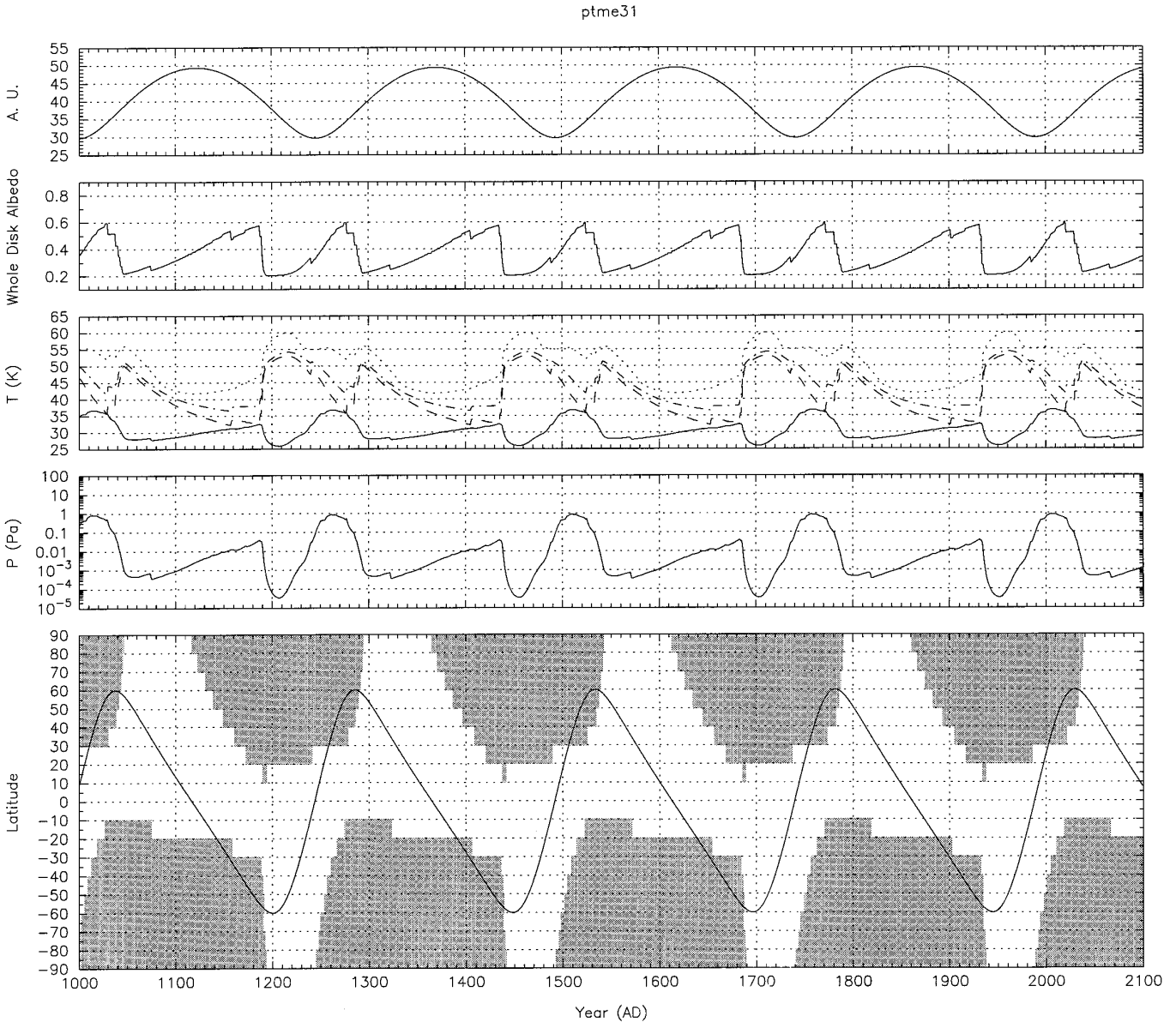


FIG. 7. Run #31, shown here, is a low thermal inertia case. This run had a thermal inertia of 1×10^{-3} cal/cm² sec^{1/2} K, a substrate albedo of 0.2, a frost albedo of 0.8, a frost emissivity of 0.8, and a nitrogen inventory of 50 kg/m². Seasonal caps without polar bald spots form. The south polar cap is still observed to persist longer than the north polar cap, but differences are not as great, because the north polar cap is able to condense earlier and sublime later than in the moderate inertia case. Atmospheric pressure variation is most pronounced for these low thermal inertia cases, with orders of magnitude difference between the maxima and minima.

run varied from 26 to 36 K. The emissivity for this run was set to 0.8, but the brightness temperature detected at 1300 μ m never dipped below the frost temperature because there was always a substantial expanse of warm substrate in view, as compared to the case illustrated in Fig. 4. Peaks in frost temperature were correlated with the subsolar latitude. Increases and decreases in the other three temperatures tracked increases and decreases in whole disk albedo.

Figure 5 shows the difference in frost distribution for high, medium, and low thermal inertia, plotted in 1945, 1965, and 1985 as Pluto would have appeared to the Earth. (North is down on this retrograde planet because Pluto observers observe the right-hand rule to define north rather than the IAU convention.) The top panel shows a high thermal inertia case with permanent zonal bands. The middle panel has low thermal inertia and seasonal caps. The bottom panel illustrates the polar bald spot which develops

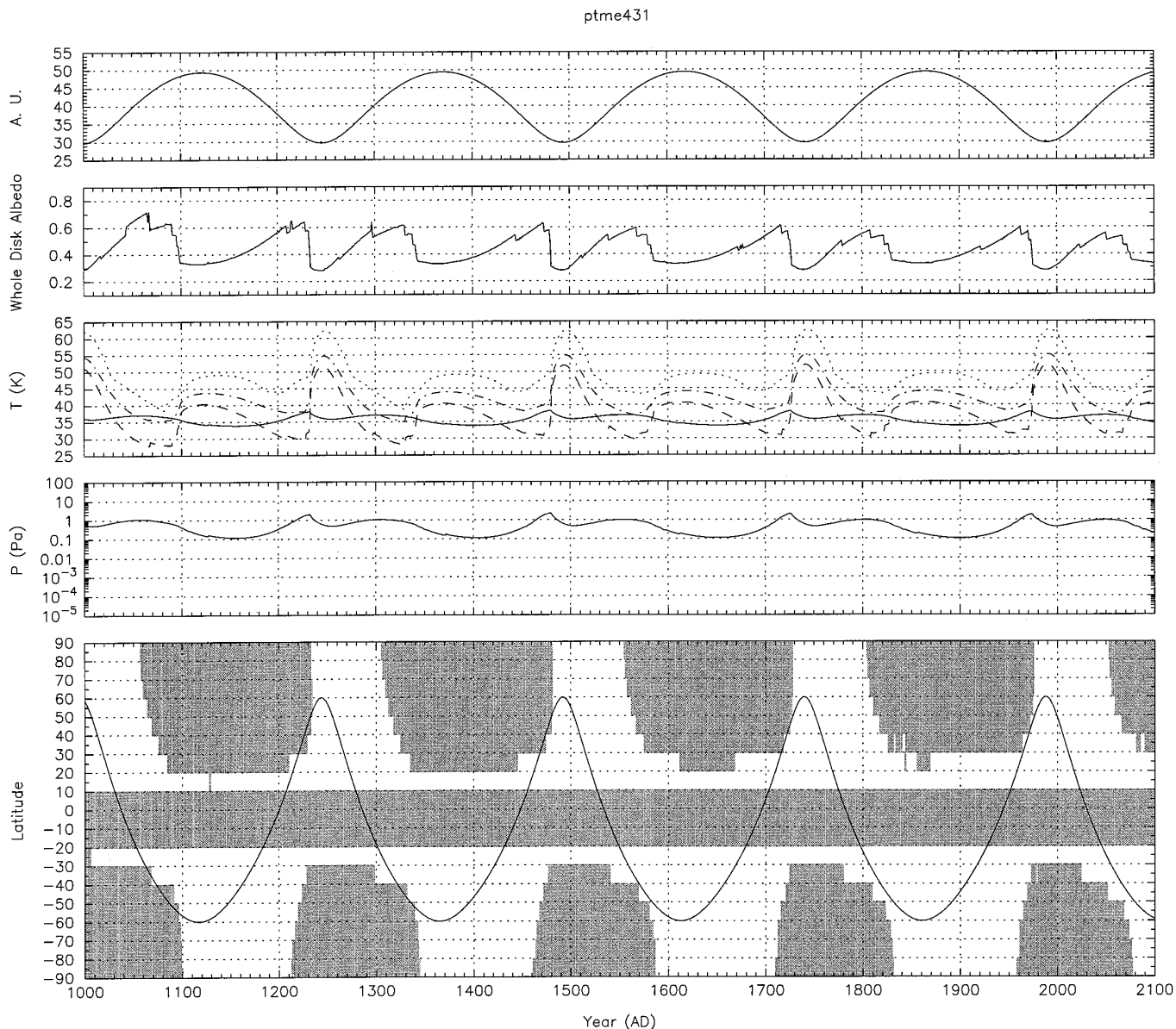


FIG. 8. Run #43 with perihelion rotated $+90^\circ$ (run #431) illustrates the effect of the precession of the longitude of perihelion on frost deposition. Pluto's high obliquity still results in the equatorial region being the permanent cold trap for volatiles, as evidenced by the permanent zonal band. This run had a thermal inertia of $7 \times 10^{-3} \text{ cal/cm}^2 \text{ sec}^{1/2} \text{ K}$, a substrate albedo of 0.2, a frost albedo of 0.8, a frost emissivity of 0.6, and a nitrogen inventory of 100 kg/m^2 . None of the runs with perihelion rotated $\pm 90^\circ$ showed formation of a permanent polar cap. Note that the time axis should be interpreted as years, not years A.D.

as frost sublimates from the pole outwards for a moderate thermal inertia case.

Emissivity

As has been noted by other authors (Stansberry *et al.* 1990, Nelson *et al.* 1990), for a given Bond albedo, an increase in frost emissivity correlates with a decrease in atmospheric pressure. High emissivity frosts are colder than low emissivity frosts. With a frost albedo of 0.8,

emissivity values lower than 0.6 predicted atmospheric pressures (associated with warm frost) far higher than the value measured during the stellar occultation in 1988. Emissivity also affected frost deposition: model runs suggest that high emissivity bright frosts won't condense as far equatorward as low emissivity frosts, and tend to condense later.

Surface emissivity was also varied for a few runs. This had the general effect of raising the substrate temperature,

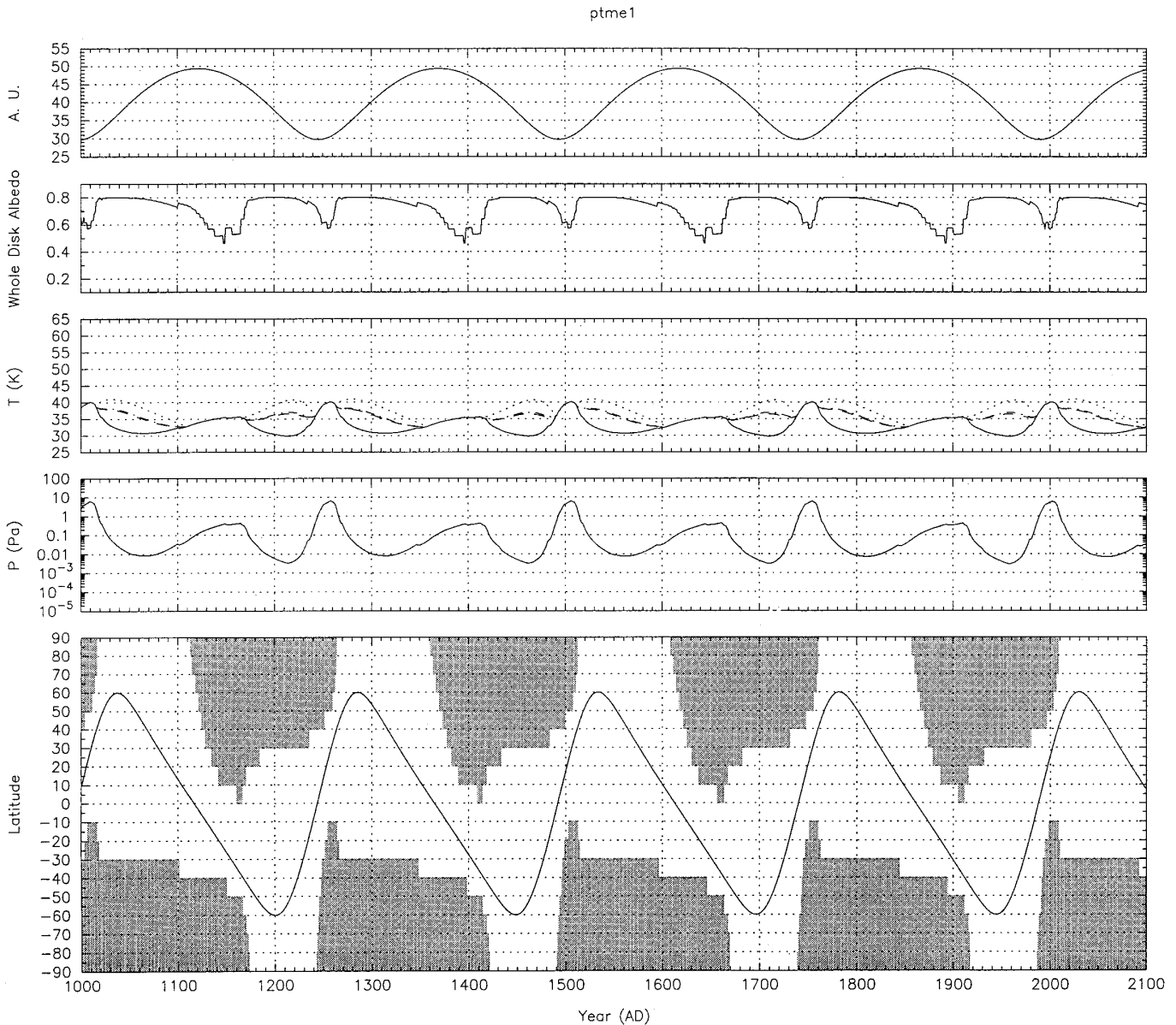


FIG. 9. This dark frost run has the best fit set of parameters for Triton: a thermal inertia of $7 \times 10^{-3} \text{ cal/cm}^2 \text{ sec}^{1/2} \text{ K}$, a substrate albedo of 0.8, a frost albedo of 0.2, a frost emissivity of 1.0, and a nitrogen inventory of 50 kg/m^2 . Although Triton observables were predicted very well by this case, it does poorly for Pluto. The frost is assumed to be dark, overlying a bright substrate. Although whole disk albedo decreased over the past 30 years, the match of albedo boundaries to observables is poor. This model run would predict that one would see not only a bright south pole, but that the entire southern hemisphere would be bright. All dark frost cases predicted formation of polar caps. Two peaks in atmospheric pressure are observed.

to the point in one particular 0.2 emissivity case that the substrate stayed too warm to permit any condensation of frost at all.

N₂ Inventory

The nitrogen inventory has a significant effect on polar cap deposits, and is one of the most poorly constrained

parameters. A large frost deposit will change temperature slowly, because of its significant heat capacity. It will take longer to go through the α - β phase transition than a thin deposit, thus delaying subsequent sublimation or condensation. This has in fact been proposed as the mechanism for maintaining a bright nitrogen polar cap on Triton, at a season when it is not expected to be stable (Duxbury and Brown 1993). Figure 6 shows a run with a global

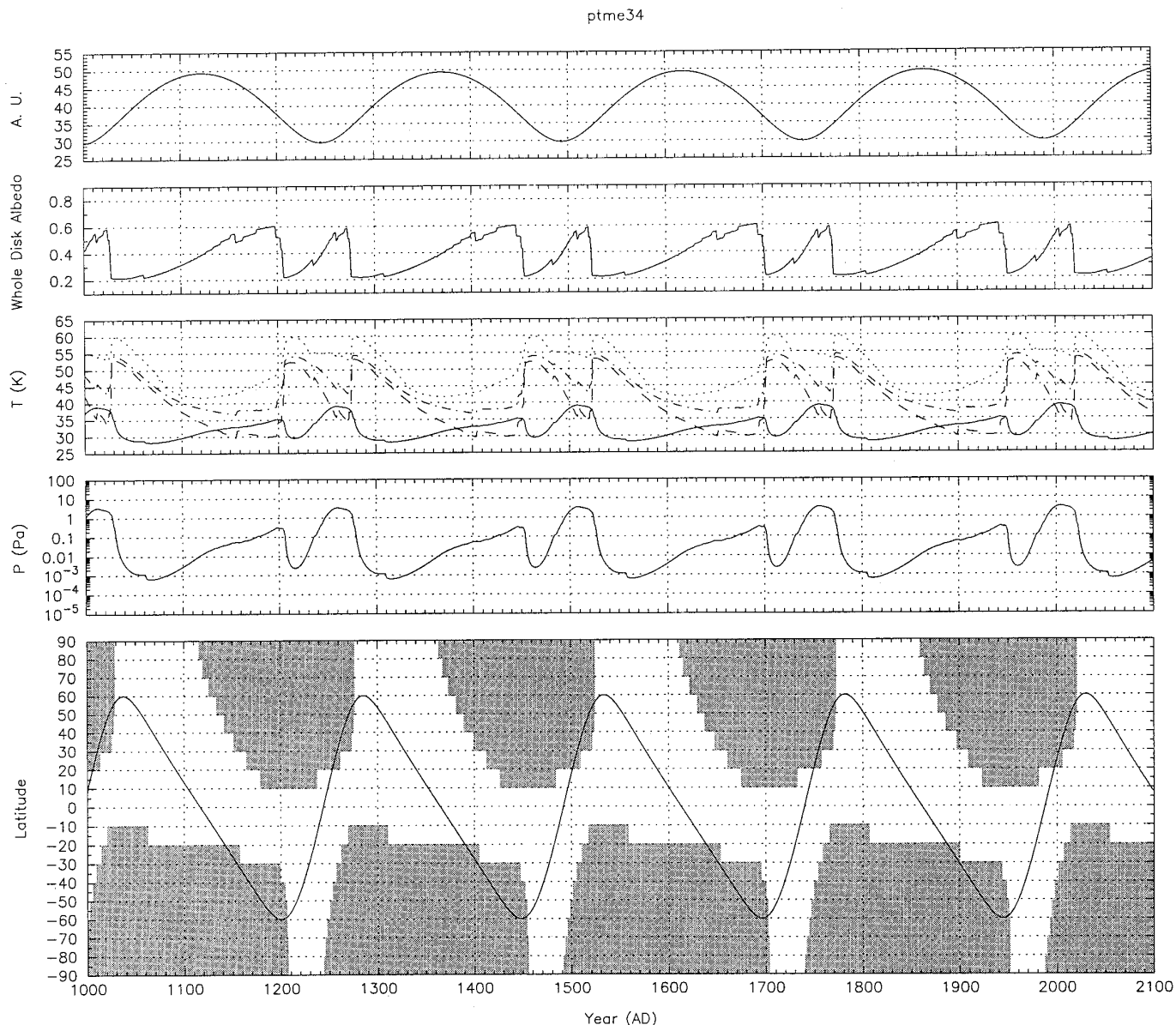


FIG. 10. This case shows a good match to albedo boundaries, but performs poorly in predicting disk-integrated albedo and atmospheric pressure. This was run #34, which had a thermal inertia of 1×10^3 cal/cm² sec^{1/2} K, a substrate albedo of 0.2, a frost albedo of 0.8, a frost emissivity of 0.6, and a nitrogen inventory of 50 kg/m².

nitrogen inventory of 100 kg/m². The only difference between the runs shown in Figs. 6 and 7 is that the nitrogen inventory was doubled. This small change caused the model to predict permanent zonal bands in addition to seasonal polar caps. As nitrogen was stabilized in the zonal band, seasonal variation in atmospheric pressure was flattened out substantially.

A nitrogen inventory in excess of that which can be moved around seasonally will eventually become sequestered in permanent cold traps. On Pluto these cold traps are currently the zonal bands. In order to analyze where

the cold trap would be, taking into account the 300 myr precession of Pluto's orbit, we ran several runs with the longitude of perihelion rotated 90°, 180°, and 270°. The result of one of these runs is shown in Fig. 8. The frost still ends up sequestered in a zonal band even with the sun shining on the north or south pole at perihelion (rather than the equator). This will be true for any volatile, thus casting doubt on Binzel's (1990) proposal that the south pole could currently be a long-term CH₄ reservoir. In the absence of a permanent asymmetry in substrate albedo or internal heating which might produce

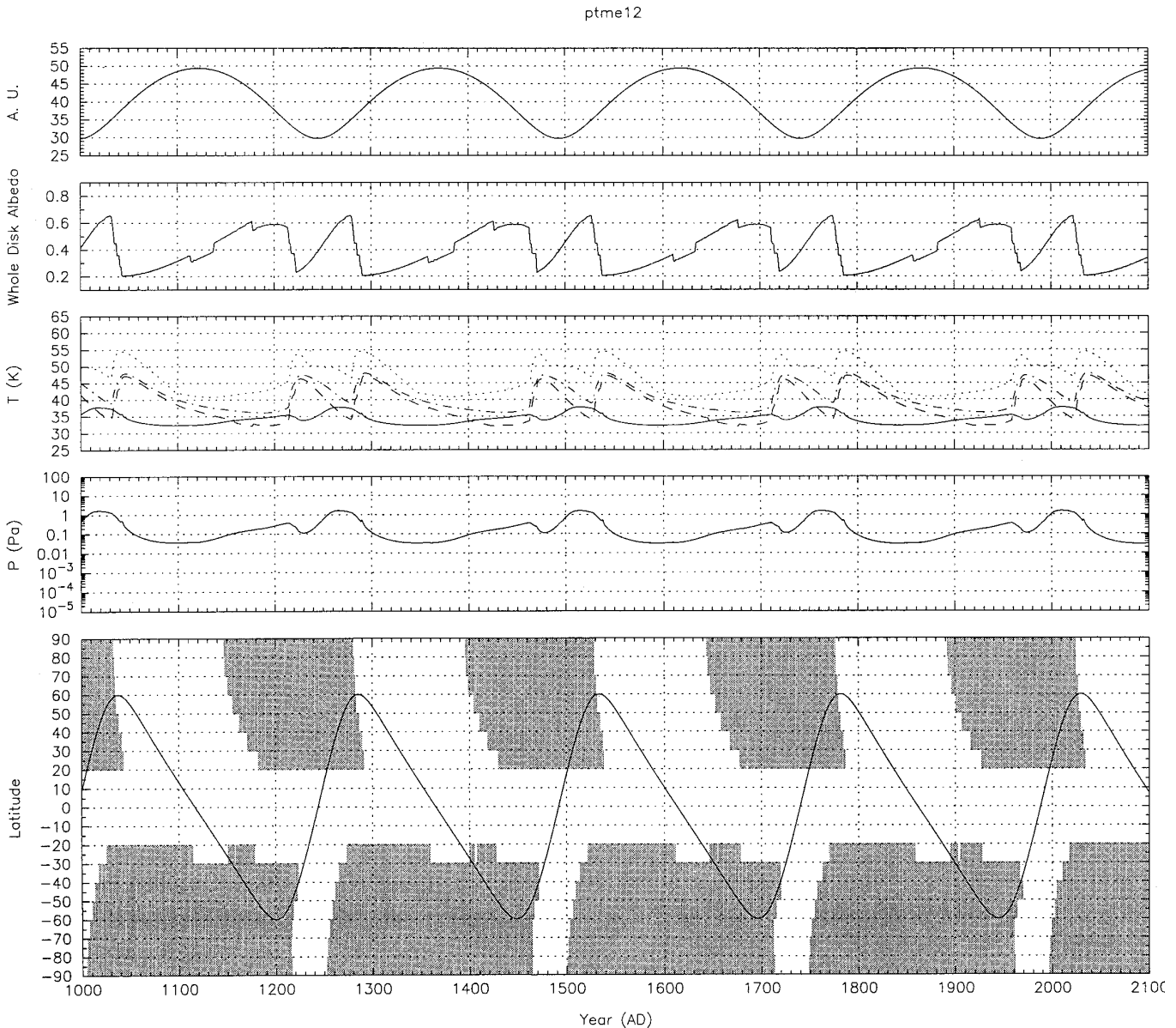


FIG. 11. This case is the best match to observables so far, although it is not perfect. This is run #12, which had a thermal inertia of 7×10^{-3} cal/cm² sec^{1/2} K, a substrate albedo of 0.2, a frost albedo of 0.8, a frost emissivity of 0.8, and a nitrogen inventory of 50 kg/m². The remnants of last Pluto year's south polar cap would have been visible in 1955, but this run does not predict formation of the new cap in time for the 1985–1988 observations of a bright south pole. It does predict dark south mid-latitudes and bright north polar cap. Whole disk albedo would have decreased from 1955 to 1970, and a recent upturn should have been observed. Atmospheric pressure was in the right ballpark in 1988, and will reach its peak in ~ 2005 . The peak will persist until ~ 2025 .

a permanent cap, the poles should only experience seasonal frost.

DISCUSSION

Bright Frost/Dark Frost Enigma

On Triton, one of the most intriguing questions raised after the Voyager flyby was “which is the polar cap—the

bright deposit seen in the southern hemisphere or the (relatively) dark northern hemisphere?”. Early thermal modeling by Stansberry *et al.* (1990), and later efforts by Hansen and Paige (1992), showed that a bright seasonal nitrogen cap would not be stable in southern summer at the time of the Voyager flyby. Spencer (1990), proposed that the nitrogen frost was relatively dark, and Eluszkiewicz (1991) proposed that freshly condensed nitrogen would be

transparent. Hansen and Paige found that a relatively dark or transparent frost yielded predictions of observables consistent with Voyager observations. These were not the only possible explanations—other possibilities included (i) a bright permanent N₂ cap produced and maintained by anisotropic internal heat flow (Brown and Kirk 1991); (ii) a permanent albedo difference of the substrate which affects the radiative balance (Moore and Spencer 1990); (iii) N₂ ice shattered by going through the α - β phase transition, and thereby changing its radiative properties (Eluszkiewicz 1991, Duxbury and Brown 1993, Tryka *et al.* 1993); and (iv) a bright lag deposit of less volatile CH₄ and possibly CO and CO₂ ices (Grundy and Fink 1991, Cruikshank *et al.* 1991, Trafton 1992).

On Pluto it is far more difficult to conceive of a process by which frost is formed which is really dark (~ 0.2 albedo), not just relatively dark (0.6 albedo). If a darkening process could be imagined, it must also be active only on Pluto and not on Triton. Dark frost runs of our model did not yield predictions at all close to Pluto's observables. Fig. 9 is a run with the parameters that gave the best fit to Triton observables. This run, as was the case with other dark frost runs, predicted that bare bright substrate would be observable from the Earth from 1955 to 1990, but that this bright ground would be visible to far above the equator, thus no dark mid-latitude band in the south was predicted. Atmospheric pressure was too high to match stellar occultation results. No differences between 60 and 1300 μm brightness temperatures were predicted. A dark frost does not rescue us on Pluto as it did on Triton, however a transparent frost cannot be ruled out. This throws more weight to the hypotheses listed above which attribute Triton's bright southern hemisphere to a permanent N₂ deposit.

Pluto's Thermal Signature

IRAS' detection of Pluto at 60 and 100 μm in 1983 led Sykes (1993) to conclude that Pluto's surface temperature was in the range 55–73 K. A warm surface could coexist with up to a projected area of 33% frost with a temperature of 35 K and be consistent with IRAS data (Sykes, 1993). This seemed to be at variance with millimeter wave measurements acquired in 1986 and in 1991, which have been interpreted to indicate a surface temperature for Pluto that is in the range 30–44 K (Altenhoff *et al.* 1988, Stern *et al.* 1993, Weintraub *et al.* 1993), unless wavelength-dependent emissivity was invoked (Sykes 1993).

Our results show that nitrogen ice will be "patchy" on a latitudinal scale (either in zonal bands or seasonal caps, but not covering the planet globally). The model predicts frost temperatures between 25 and 40 K, depending on the emissivity, and maximum surface temperatures for unfrosted areas to be in the 50 to 60 K range, depending on substrate thermal inertia. Our model predicts that the

temperature measured at the earth depends significantly on the viewing geometry from the Earth. Figure 4, for example, showed a case in which at times, although the surface was much warmer, the viewing geometry was such that the measurement made from the Earth would be the temperature of the polar cap frost. Furthermore, the brightness temperature measured at 60 and at 1300 μm is a function of time, as frost and surface physical temperatures change and the frost moves around. In 10 years as much as a 15 K difference in brightness temperatures at these wavelengths can arise from the combination of temporal changes in surface and frost temperatures and the change in viewing geometry.

Match To Observables

As was the case for Triton, the observed albedo boundaries are not easy to match. We do not find in any of our runs a bright nitrogen cap that would persist from 1955 through 1990. We do see cases in which an old south polar cap is still in place in 1955, subsequently sublimates, and a new south polar cap has begun to condense by 1980. The bright north polar cap comes into view as the subsolar latitude approaches the equator. This situation would potentially yield a bright south pole and dark south mid-latitudes with a bright northern hemisphere. The low thermal inertia case illustrated in Fig. 10 shows an example of this case, but the atmospheric pressure and albedo trends are not good matches to data.

A high thermal inertia substrate with just a permanent zonal band (no seasonal caps) can be ruled out because predicted albedo markings are completely inconsistent with observations. A dark frost case can be discarded for reasons given above.

The best match so far to Pluto observables is shown in Fig. 11. This run had a moderate thermal inertia, a frost emissivity of 0.8, and a nitrogen inventory of 50 kg/m². This case still had a bright south polar cap in 1955, and a bright northern cap rotating into view in the 1980s, coarsely consistent with the trends derived by Drish *et al.* (1995) and certainly consistent with the HST images obtained in 1994 by Stern *et al.* (1995). The run showed a decrease in disk-integrated albedo as seen from the Earth between 1955 and 1970. This case is flawed in that it does not predict any frost still in the southern hemisphere at the time of the mutual occultations, and model predictions give an upturn in disk-integrated albedo earlier than that observed (Drish *et al.* 1995). The atmospheric pressure is in the right ballpark. The brightness temperature measured at 60 μm from the Earth in 1983 was predicted to be 48 K, significantly lower than the 54 K value measured by IRAS, while the prediction for 1300 μm in 1991 was 42 K, a close match to the microwave observations.

Multicomponent Ices

Our model only considers N_2 ice. It is reasonable to ask whether less volatile CH_4 could be responsible for the bright south polar deposit so clearly observed in 1955. Owen *et al.* (1993) have made the case that the best fit to their spectral data is the situation in which N_2 is in solid solution with CH_4 and CO , in an intimate, if not molecular, mixture. The spectral data thus argues against large lag deposits of less volatile ice. On the other hand, one would expect that the differing volatility of these substances would tend to “distill” these ices seasonally (Trafton 1990, Stansberry *et al.* 1990). Young *et al.* (1993) have shown that Pluto’s methane signature is enhanced in their data near the south pole.

This appears to be an exciting area for more research and analysis. It would be very interesting to replace the vapor pressure equilibrium curve our model uses currently with an appropriate, evolving multicomponent set of lookup tables. We could then ask the following questions: How might the observed spectra of Pluto evolve seasonally? Will ices on the surface always appear to be intimately mixed? Will layering of different ices develop? Will one mask the signature of another as they move around? Can we gain more insight into the composition and thermal structure as a function of altitude of the atmosphere, by tracking the diffusion of CH_4 , not just on the surface but also in the atmosphere? How is the current inventory different from the primordial, taking into account seasonal loss to space (Trafton, 1990)?

The ability of our model to track the spatial distribution of mass as it moves around seasonally is key to addressing this set of issues. “Mass” currently means “nitrogen” to the model. It can track both α and β ices. It will require careful but not impossible changes to the code to add other volatiles, and we think the results of this endeavor will be exciting and worthwhile.

CONCLUSIONS

Application of the Triton thermal model to Pluto has enabled comparisons of the seasonal nitrogen cycles on these two bodies. Although they may have formed in the same region of the solar system and share many similarities, their climates today depend most significantly on their current orbital characteristics. Trends have been identified as frost and substrate properties have been varied. We have not yet found a uniform set of parameters which could yield good matches to observables for both bodies.

The failure to find a set of parameters which match all Pluto observables does not necessarily mean that the assumption of vapor pressure equilibrium was flawed. It does indicate that the situation is more complex than can be described by a simple thermal model. Multicomponent ices certainly play a role. Time variability of frost proper-

ties may be an important factor. Application of a simple model is just the first step in the process of understanding the real Pluto climate, and trends identified will lead to insight into more complex processes that must be incorporated for the model to be viable.

We have shown that Pluto’s eccentric orbit and high obliquity have a very significant effect on the condensation and sublimation of its polar caps. The eccentricity of Pluto’s orbit is the reason that the northern cap condenses slowly as Pluto moves through aphelion, whereas the southern cap condenses quickly as the sun moves to its most northerly latitude just after perihelion. In many cases the southern cap persists longer than the northern cap because of its slow rate of sublimation. Pluto’s high obliquity is responsible for the prediction of the formation of zonal bands in high thermal inertia cases, and polar bald spots in moderate thermal inertia runs. Pluto’s equatorial region is found to be the long-term cold trap for volatiles, even in the epoch when the longitude of perihelion is rotated $\pm 90^\circ$.

Differences between brightness temperatures measured at infrared and millimeter wavelengths are to be expected. Model results indicate that differences will result from the change in time between the measurements, attributable to the combination of change in viewing geometry, redistribution of frost, and change in frost and substrate physical temperatures over the intervening years. The warmest substrate surface temperatures we predict are 60 K for a low thermal inertia run and 50 K for a high thermal inertia run. Frost physical temperature ranged from 25 to as high as 40 K, depending on frost parameters assumed.

The atmospheric pressure variations are of perhaps the most interest in planning for future Pluto missions. We find that in most cases the high levels of atmospheric pressure that Pluto is currently experiencing will continue to increase until the year 2000, but will start to drop after 2020. The pressure may drop by many orders of magnitude, and the drop to low pressure will persist through Pluto’s slow excursion through aphelion.

Pluto observables supply an additional set of constraints on frost properties on both Triton and Pluto, and to date, a satisfactory match to all observables on both bodies has not been found. The chief discrepancy is the inability of bright volatile nitrogen frost to persist through the southern spring and summer.

Our model philosophy has been to avoid all ad hoc assumptions, no matter how feasible. For example, all variables are constant once a run has been initialized—they are not a function of latitude or time. It is certainly feasible that these parameters vary temporally or spatially, but because of the exploratory nature of our studies, and the lack of data, we thought it best to keep them constant. Our research and that of other investigators has suggested areas in which this strict philosophy might fruitfully be relaxed now. The true complexity of the environment on

Triton and Pluto appears to require a more complicated approach.

Our future work will focus on these possibilities: (i) A large CH₄ deposit, subliming more slowly than the seasonal N₂ frost, can be invoked to explain lightcurve observations, but it will ultimately have to be consistent with spectral observations as well; (ii) With the addition of the α - β phase to our model, we are in a position to test the explanation proposed by Duxbury and Brown (1993), in which a large inventory of nitrogen frost is stabilized by the α - β transition; (iii) Modeling of transparent frost cases, in which frost is assigned the albedo of the underlying substrate (which may be assigned differing values latitudinally), is straightforward because the model does not differentiate between heat absorbed at the top or at the bottom of the frost layer; (iv) The assumption of isotropic internal heating will be relaxed to study the radiative effect of a permanent difference in substrate albedo that would be due to a permanent deposit stabilized thermally against eventual transport.

ACKNOWLEDGEMENTS

Very helpful comments were received from Larry Trafton, Mark Sykes, and John Spencer. The research described in this paper was carried out at the Jet Propulsion Laboratory, California Institute of Technology, under a contract with the National Aeronautics and Space Administration, under the auspices of the Neptune Data Analysis Program.

REFERENCES

- ALTENHOFF, W. J., R. CHINI, H. HEIN, E. KREYSA, P. G. MEZGER, C. SALTER, AND J. B. SCHRAML 1988. First radio astronomical estimate of the temperature of Pluto. *Aston. Astrophys.* **190**, L15-L17.
- BINZEL, R. P. 1990. *Lunar Planet. Sci. Conf.* **21**, 87-88.
- BROADFOOT, L., S. ATREYA, J. BERTAUX, J. BLAMONT, A. DESSLER, T. DONAHUE, W. FORRESTER, D. HALL, F. HERBERT, J. HOLBERG, D. HUNTEN, V. KRASNOPOLSKY, S. LINICK, J. LUNINE, J. MCCONNELL, H. MOOS, B. SANDEL, N. SCHNEIDER, D. SHEMANSKY, G. SMITH, D. STROBEL, AND R. YELLE 1989. Ultraviolet spectrometer observations of Neptune and Triton. *Science* **246**, 1459-1465.
- BROWN, G. N., AND W. T. ZIEGLER 1980. Vapor pressure and heats of vaporization and sublimation of liquids and solids of interest in cryogenics below 1-atm pressure. *Adv. Cryogen. Eng.* **25**, 662-670.
- BROWN, R. H., T. JOHNSON, J. GOGUEN, G. SCHUBERT, AND M. ROSS 1991. Triton's global heat budget. *Science* **251**, 1465-1467.
- BROWN, R. H. AND R. L. KIRK 1991. Coupling of internal heat to volatile transport on Triton. *Bull. Am. Astron. Soc.* **23**, 1210.
- BUIE, M. W., D. J. THOLEN, AND K. HORNE 1992. Albedo maps of Pluto and Charon: Initial mutual event results *Icarus* **97**, 211-227.
- CRUIKSHANK, D. P., C. B. PILCHER, D. MORRISON 1976. Pluto: Evidence for methane frost. *Science* **194**, 835-837.
- CRUIKSHANK, D., R. H. BROWN, AND R. CLARK 1984. Nitrogen on Triton. *Icarus* **58**, 293-305.
- CRUIKSHANK, D. P., T. OWEN, T. GEBALLE, B. SCHMITT, C. DE BERGH, J.-P. MAILLARD, B. LUTZ, AND R. H. BROWN 1991. Tentative detection of CO and CO₂ ices on Triton. *Bull. Am. Astron. Soc.* **23**, 1208.
- CRUIKSHANK, D. P., T. L. ROUSH, T. C. OWEN, T. R. GEBALLE, C. DE

- BERGH, B. SCHMITT, R. H. BROWN, AND M. J. BARTHOLOMEW 1993. Ices on the surface of Triton. *Science* **261**, 742-745.
- DRISH, W. F. JR., R. HARMON, R. L. MARCIALIS, AND W. J. WILD 1995. Images of Pluto generated by matrix lightcurve inversion. *Icarus* **113**, 360-386.
- DUXBURY, N. S., AND R. H. BROWN 1993. The phase composition of Triton's polar caps. *Science* **261**, 748-751.
- ELLIOT, J. L., E. W. DUNHAM, A. S. BOSH, S. M. SLIVAN, AND L. A. YOUNG 1989. Pluto's radius and atmosphere: Results from the entire 9 June 1988 occultation data set. *Icarus* **77**, 148-170.
- ELLIOT, J. L. AND L. A. YOUNG 1992. Analysis of stellar occultation data for planetary atmospheres. I. Model fitting with application to Pluto. *Astron. J.* **103**, 991-1015.
- ELUSZKIEWICZ, J. 1991. On the microphysical state of the surface of Triton. *J. Geophys. Res.* **96**, 217-231.
- GRUNDY, W. M., AND U. FINK 1991. A new spectrum of Triton near the time of the Voyager encounter. *Icarus* **93**, 379-385.
- HANSEN, C. J. AND D. A. PAIGE 1992. A thermal model for the seasonal nitrogen cycle on Triton. *Icarus* **99**, 273-288.
- HUBBARD, W. B., R. V. YELLE, AND J. I. LUNINE 1990. Nonisothermal Pluto atmosphere models. *Icarus* **84**, 1-11.
- HUNTEN, D. M., AND A. J. WATSON 1982. Stability of Pluto's atmosphere. *Icarus* **51**, 665-667.
- INGERSOLL, A. 1989. Io meteorology: How atmospheric pressure is controlled locally by volcanos and surface frosts. *Icarus* **81**, 298-313.
- JOHNSON, V., Ed. 1960. A compendium of the properties of materials at low temperature (part 1). Wadd Technical Report 60-56.
- LEIGHTON, R. AND B. MURRAY 1966. Behavior of carbon dioxide and other volatiles on Mars. *Science* **153**, 136-144.
- LUPO, M. J. AND J. S. LEWIS, 1980. Mass-radius relationships and constraints on the composition of Pluto. *Icarus* **42**, 29-34.
- MOORE, J. M., AND J. R. SPENCER 1990. Koyaanismuyaw: The hypothesis of a perennially dichotomous Triton. *Geophys. Res. Lett.* **17**, 1757-1760.
- MORRISON, D. AND D. P. CRUIKSHANK 1973. Thermal properties of the Galilean satellites. *Icarus* **18**, 224-236.
- NELSON, R. M., W. D. SMYTHE, B. D. WALLIS, L. J. HORN, A. L. LANE, AND M. J. MAYO 1990. Temperature and thermal emissivity of the surface of Neptune's satellite Triton. *Science* **250**, 429-431.
- NULL, G. W., W. M. OWEN, JR., AND S. P. SYNNOTT 1993. Masses and densities of Pluto and Charon. *Astron. J.* **105**, 2319-2335.
- OWEN, T. C., T. GEBALLE, C. DE BERGH, L. YOUNG, J. ELLIOT, D. CRUIKSHANK, T. ROUSH, B. SCHMITT, R. H. BROWN, AND J. GREEN 1992. Detection of nitrogen and carbon monoxide on the surface of Pluto. *Bull. Am. Astron. Soc.* **24**, 961.
- OWEN, T. C., T. L. ROUSH, D. P. CRUIKSHANK, J. L. ELLIOT, L. A. YOUNG, C. DE BERGH, B. SCHMITT, T. R. GEBALLE, R. H. BROWN, AND M. J. BARTHOLOMEW 1993. Surface ices and the atmospheric composition of Pluto. *Science* **261**, 745-748.
- PAIGE, D. 1992. The thermal stability of near-surface ground ice on Mars. *Nature* **356**, 43-45.
- SPENCER, J. 1990. Nitrogen frost migration on Triton: A historical model. *Geophys. Res. Lett.* **17**, 1769-1772.
- SPENCER, J. R. AND J. M. MOORE 1992. The influence of thermal inertia on temperatures and frost stability on Triton. *Icarus* **99**, 261-272.
- STANSBERRY, J., J. LUNINE, AND C. PORCO 1990. Zonally averaged thermal balance and stability models for nitrogen polar caps on Triton. *Geophys. Res. Lett.* **17**, 1773-1776.
- STERN, S. A. AND L. TRAFTON 1984. Constraints on bulk composition, seasonal variation, and global dynamics of Pluto's atmosphere. *Icarus* **57**, 231-240.

- STERN, S. A., L. M. TRAFTON, G. R. GLADSTONE 1988. Why is Pluto bright? Implications of the albedo and lightcurve behavior of Pluto. *Icarus* **75**, 485–498.
- STERN, S. A. 1991. On the number of planets in the outer Solar System: Evidence of a substantial population of 1000-km bodies. *Icarus* **90**, 271–281.
- STERN, S. A., D. A. WEINTRAUB, M. C. FESTOU 1993. Evidence for a low surface temperature on Pluto from millimeter-wave thermal emission measurements. *Science* **261**, 1713–1716.
- STERN, S. A., M. W. BUIE, L. M. TRAFTON, AND B. C. FLYNN 1995. High resolution HST images of the Pluto–Charon system. *Lunar Planet Sci. Conf.* **XXVI**, 1359–1360.
- SYKES, M., R. CUTRI, L. LEBOSKY, AND R. BINZEL 1987. IRAS serendipitous survey observations of Pluto and Charon. *Science* **237**, 1336–1340.
- SYKES, M. 1993. Implications of Pluto–Charon radiometry. *Bull. Am. Astron. Soc.* **25**, 1138.
- TRAFTON, L. AND S. A. STERN 1983. On the global distribution of Pluto's atmosphere. *Astrophys. J.* **267**, 872–881.
- TRAFTON, L. 1984. Large seasonal variations in Triton's atmosphere. *Icarus* **58**, 312–324.
- TRAFTON, L. 1990. A two-component volatile atmosphere for Pluto. I. The bulk hydrodynamic escape regime. *Astrophys. J.* **359**, 512–523.
- TRAFTON, L. M. 1992. Methane enhancement in Triton's south polar cap: Interpretation in terms of CH₄ and N₂ in solid solution. Neptune and Triton Conference Abstract.
- TRYKA, K. A., R. H. BROWN, V. ANICICH, D. P. CRUIKSHANK, T. C. OWEN 1993. Spectroscopic determination of the phase composition and temperature of nitrogen ice on Triton. *Science* **261**, 751–754.
- TYLER, G., D. SWEETNAM, J. ANDERSON, S. BORUTZKI, J. CAMPBELL, V. ESHLEMAN, D. GRESH, E. GURROLA, D. HINSON, N. KAWASHIMA, E. KURSINSKI, G. LEVY, G. LINDAL, J. LYONS, E. MAROUF, P. ROSEN, R. SIMPSON, AND G. WOOD 1989. Voyager radio science observations of Neptune and Triton. *Science* **246**, 1466–1473.
- WARD, W. R. 1974. Climatic variations on Mars: 1. Astronomical theory of insolation *J. Geophys. Res.* **79**, 3375–3386.
- WEINTRAUB, D. A., S. A. STERN, AND M. C. FESTOU 1993. Millimeter-wave measurements of Pluto's thermal emission: Evidence for a cold surface. Pluto and Charon Conference abstract, p. 72.
- YOUNG, E. F. AND R. P. BINZEL 1993. Comparative mapping of Pluto's sub-Charon hemisphere: Three least squares models based on mutual event lightcurves. *Icarus* **102**, 134–149.
- YOUNG, E. F., M. W. BUIE, D. P. CRUIKSHANK 1993. Four IR maps of Pluto and their usefulness in identifying methane concentrations. Pluto and Charon Conference Abstracts, p. 77.